DsrMKJOP is the terminal reductase complex in anaerobic sulfate respiration

Ana C. C. Barbosa[‡], Sofia S. Venceslau[‡]*, Inês A. C. Pereira*

Instituto de Tecnologia Química e Biológica António Xavier, Universidade Nova de Lisboa, 2780-156 Oeiras, Portugal

[‡]These authors contributed equally to this work

*Corresponding authors: ipereira@itqb.unl.pt, sofiasvenceslau@gmail.com

A.C.C.B.: ORCID ID: 0000-0003-3577-2927

S.S.V.: ORCID ID: 0000-0001-8774-1351

I.A.C.P.: ORCID ID: 0000-0003-3283-4520

KEYWORDS

Dissimilatory sulfur metabolism, sulfate reducers, DsrAB/C, DsrMKJOP

The authors have no competing interests.

ABSTRACT

Microbial dissimilatory sulfate reduction is a key process in the Earth biogeochemical sulfur cycle. In spite of its importance to the sulfur and carbon cycles, industrial processes and human health, it is still not clear how reduction of sulfate to sulfide is coupled to energy conservation. A central step in the pathway is the reduction of sulfite by the DsrAB dissimilatory sulfite reductase, which leads to the production of a DsrC-trisulfide. The involvement of the membrane-bound DsrMKJOP complex in the production of sulfide has been inferred from sequence analysis, but its precise function was so far not determined. Here, we present biochemical studies revealing that the DsrMKJOP complex of *Archaeoglobus fulgidus* works as a menadiol:DsrC-trisulfide oxidoreductase. Our results confirm a close interaction between the DsrC-trisulfide and the DsrMKJOP complex and show that electrons flow from menadiol to DsrM hemes *b*, to DsrK noncubane $[4Fe\text{-}4S]^{3+/2+}$ catalytic center, and finally to the DsrC-trisulfide with concomitant release of sulfide. These results clarify the role of this widespread respiratory membrane complex and indicate that DsrMKJOP can provide the missing link to energy conservation by generating a *proton motive force* across the membrane in the last step of dissimilatory sulfate reduction.

36 **INTRODUCTION**

37 Sulfur is a key element for life, mainly due to its chemical versatility and ability to switch between several
38 biologically relevant oxidation states, ranging from -2, as in hydrogen sulfide (H_2S), up to +6, as in sulfate
39 (SO_4^{2-}). A critically important microbial process in the biogeochemical sulfur cycle is dissimilatory sulfate
40 reduction (DSR) driven by anaerobic bacteria and archaea, in which the reduction of sulfate to hydrogen
41 sulfide is linked to energy conservation [1, 2]. This process has particular impact in marine sediments,
42 accounting for up to 50% of carbon mineralization in the sea floor [3], and preventing methane emissions
43 through its contribution to anaerobic methane oxidation [4, 5]. Despite being a very ancient bioenergetic
44 pathway [6], it is still not clear how sulfate reducers are able to conserve energy during sulfate respiration.
45 In DSR, a central step is the reduction of sulfite, performed by the dissimilatory sulfite reductase DsrAB
46 and its physiological partner DsrC, which mediate a four-electron reduction of sulfite to zero-valent sulfur
47 in the form of a trisulfide formed between two conserved cysteines of DsrC [7, 8]. The reduction of the
48 DsrC-trisulfide to hydrogen sulfide is thought to derive electrons from the quinone pool via the
49 membrane-bound DsrMKJOP complex, pointing to a critical role of this complex in energy conservation
50 [7, 9, 10]. The Dsr proteins, namely DsrAB, DsrC and DsrMKJOP, are widespread in the microbial world,
51 being also present in phototrophic and chemotrophic sulfur-oxidizing organisms where they are involved
52 in sulfite oxidation [11, 12], and in many organisms capable of sulfur, thiosulfate, sulfite or
53 organosulfonates reduction, and in sulfur disproportionators [13, 14]. However, there is still no concrete
54 evidence demonstrating the physiological function of the DsrMKJOP complex.

55 The DsrMKJOP complex was first isolated and characterized from *Archaeoglobus fulgidus* [15], then from
56 *Desulfovibrio desulfuricans* [10], and later from *Allochromatium vinosum* [16], where this complex has
57 been shown to be essential for sulfur globule oxidation [17]. This transmembrane complex contains two
58 periplasmic subunits (DsrJ and DsrO), two integral membrane subunits (DsrM and DsrP) and a cytoplasmic
59 subunit (DsrK), and appears to be composed of a combination of two modules, DsrMK and DsrJOP [18].

60 The MK module is homologous to the membrane-bound HdrED heterodisulfide reductase (Hdr) from
61 methanogens [19–21], comprising a quinone-interacting membrane diheme cytochrome *b* DsrM, with
62 both hemes displaying His/His coordination, and an iron-sulfur subunit DsrK predicted to have two
63 canonical $[4Fe\text{-}4S]^{2+/1+}$ clusters, and one noncubane $[4Fe\text{-}4S]^{3+/2+}$ cluster [10]. The noncubane cluster is
64 predicted on the basis of a conserved five-cysteine motif $CX_nCCGX_nCX_2C$ (the CCG motif) [22], which was
65 identified to bind the catalytic noncubane cluster for heterodisulfide reduction in the homologous HdrD
66 [15]. The DsrJOP module contains DsrP, an integral membrane subunit with ten predicted transmembrane
67 helices, and DsrO, an iron-sulfur subunit predicted to coordinate three to four $[4Fe\text{-}4S]^{2+/1+}$ clusters, which
68 together resemble the quinone-interacting NrfCD module widespread in bacterial oxidoreductases [23].
69 DsrJ is a membrane-anchored triheme cytochrome *c*, where each heme is proposed to have distinct axial
70 coordination: His/His, His/Met and His/Cys [10, 24]. The His/Cys heme *c* coordination is very unusual but
71 is also found in SoxXA [25], TdsA [26] and PufC [27], which are involved in thiosulfate oxidation and/or
72 electron transfer, suggesting that DsrJ could have a catalytic role in sulfur redox chemistry. Notably, the
73 DsrJOP module is absent in many Gram-positive (Firmicutes) and archaeal sulfate reducers [18], and so
74 does not seem to be essential. In contrast, the DsrMK proteins are present in all organisms containing
75 DsrAB and DsrC, often encoded in the same operon and sometimes with multiple copies in the genome,
76 which suggests this is the minimum functional module of this respiratory complex [18]. Based on its
77 similarity to HdrED, the DsrMK module was proposed to catalyze the reduction of DsrC-trisulfide to
78 hydrogen sulfide through the oxidation of the quinone pool [7, 9, 10, 28]. However, the presence of the
79 DsrJOP module suggests that there may be a more elaborate mechanism [7]. Both DsrM and DsrP are
80 homologous to quinone-interacting proteins, and the presence of two putative quinone-binding sites led
81 to the suggestion that a quinone cycle between the DsrMK and DsrJOP modules may be present [9].
82 The X-ray structure of the soluble HdrABC-MvhAGD complex from the methanogenic archaeon
83 *Methanothermococcus thermolithotrophicus*, comprising the MvhAGD hydrogenase and the HdrABC

84 heterodisulfide reductase, provided the first structural insights into the two noncubane $[4Fe\text{-}4S]^{3+/2+}$
85 clusters present in the active site of HdrB, and how they mediate the reduction of CoM-S-S-CoB
86 heterodisulfide [29]. Each noncubane cluster is ligated by five cysteines from the predicted CCG motif.
87 There are two such motifs in both HdrB and HdrD, the catalytic subunits of the two different types of Hdrs
88 in methanogens. Cleavage of the CoM-S-S-CoB disulfide bond has been suggested to involve the two
89 noncubane clusters in a homolytic mechanism, along with binding of each substrate to one of the clusters
90 [29]. Remarkably, only one CCG motif is present in DsrK, raising the question of how this protein may
91 operate with a single noncubane cluster. Recently, studies of the noncubane $[4Fe\text{-}4S]^{3+/2+}$ cluster in the
92 HdrB protein from *Desulfovibrio vulgaris* Hildenborough revealed that this cluster can adopt "closed" and
93 "open" conformations corresponding to the substrate-free and substrate-bound forms, respectively [30],
94 suggesting that cluster flexibility may be important for binding the DsrC-trisulfide in the active site of its
95 homolog, DsrK.
96 Overall, unraveling the role of the DsrMKJOP complex and its link to DsrC-trisulfide reduction and
97 corresponding energy conservation mechanism is a major challenge in understanding dissimilatory sulfur
98 metabolism. In the present study, we provide evidence for the activity of the DsrMKJOP complex as a
99 menadiol:DsrC-trisulfide oxidoreductase, clarifying the functional role of this membrane complex in the
100 final step of the sulfate respiratory chain, where it is likely coupled to energy conservation.
101

102 **MATERIALS AND METHODS**

103 **Purification of *A. fulgidus* DsrMKJOP**

104 *A. fulgidus* VC-16 (DSM 4304) was grown in sulfate-thiosulfate-lactate medium in 300 L fermenter at 83
105 °C, as previously described [31], without addition of dithionite. Frozen cells were resuspended in 50 mM
106 potassium phosphate buffer (KPi) pH 7.0, 10% (v/v) glycerol, homogenized and disrupted in an APV Model
107 2000 Homogenizer at 80 MPa in the presence of DNase (Sigma-Aldrich) and cOmplete™ protease inhibitor

108 cocktail (Roche). The cell lysate was centrifuged at 7930 x *g* for 20 min at 4 °C, followed by
109 ultracentrifugation at 138000 x *g* for 2 h at 4 °C. The supernatant (soluble extract) was used to isolate *A.*
110 *fulgidus* DsrAB (see below). The pellet (membrane extract) was solubilized with gentle stirring overnight
111 at 4 °C in 50 mM potassium phosphate buffer pH 7.0, 10% (v/v) glycerol, and 2% (w/v) n-dodecyl β-D-
112 maltoside (DDM, Glycon Biochemicals GmbH). The solubilized membrane proteins were separated by
113 ultracentrifugation at 138000 x *g* for 2 h at 4 °C, and the membrane pellet was used for a second
114 solubilization for 5 h with gentle stirring at 4 °C, followed by a third ultracentrifugation step under the
115 same conditions. The pooled solubilized membrane proteins were loaded into a Q-Sepharose high
116 performance column (2.6 x 10.0 cm, Amersham Pharmacia Biotech) equilibrated with buffer A (50 mM
117 KPi pH 7.0, 10% (v/v) glycerol, 0.1% (w/v) DDM, and a cOmplete^{TM} protease inhibitor tablet/L). A stepwise
118 gradient of increasing concentrations of NaCl (from 0 to 1 M NaCl) was applied and the fractions eluted
119 at 0.45 M and 0.5 M NaCl were pooled, concentrated and the ionic strength of the solution was lowered
120 by dilution with buffer A and ultrafiltration (50 kDa cutoff, Amicon, Millipore). The concentrate was
121 applied to a Resource Q column (1.6 x 3.0 cm, Amersham Pharmacia Biotech) equilibrated with buffer A.
122 A stepwise gradient of increasing concentrations of NaCl (from 0 to 1 M NaCl) was performed and the
123 fractions eluted at 0.3 M and 0.35 M NaCl were pooled, concentrated and the ionic strength lowered by
124 dilution and concentration steps as above. All the chromatographic steps were performed at 4 °C, at air,
125 and monitored by UV-visible spectroscopy. The purity of DsrMKJOP was analyzed by a 10% Tricine-SDS-
126 PAGE gel and a Blue Native (BN)-PAGE gel, followed by Coomassie Blue staining and heme-staining [32],
127 and the protein concentration was determined using the previously determined absorption coefficient (ε)
128 of 132.4 $mM^{-1}.cm^{-1}$ at 555 nm in the reduced state [33].

129 **UV-visible Spectroscopy**

130 UV–visible spectra were acquired in a Shimadzu UV-1800 spectrophotometer inside a Coy anaerobic
131 chamber (98 % N_2, 2 % H_2). Spectra were obtained at 60 °C, using as-purified DsrMKJOP, prepared in 20

132 mM Tris-HCl pH 7.5, then incubated with menadiol and an excess of sodium dithionite to allow full
133 reduction. Menadiol was prepared by reduction of menadione with sodium dithionite [34], stored in dry
134 state at -20 °C under anaerobic conditions, and solubilized in ethanol prior to use. A control spectrum of
135 the as-purified DsrMKJOP complex was obtained by addition of the same volume of ethanol as for
136 menadiol incubation.
137
138 **Electron Paramagnetic Resonance Spectroscopy**
139 X-band electron paramagnetic resonance (EPR) spectra were obtained on a Bruker EMX spectrometer
140 (Billerica, MA) equipped with an Oxford Instruments ESR-900 continuous flow helium cryostat (Abingdon,
141 UK). A menadiol-treated sample of the DsrMKJOP complex, in 20 mM Tris-HCl pH 7.5 at a concentration
142 of 25 µM, was prepared inside a Coy anaerobic chamber (98 % N_2, 2 % H_2) by incubation for 2h at 60 °C
143 with a solution of menadiol in ethanol in a 1:500 ratio. As control an as-purified DsrMKJOP sample was
144 also incubated for 2 h with the same volume of ethanol as was used in the menadiol experiment. Samples
145 were transferred to EPR tubes within the anaerobic chamber, capped, and immediately frozen in liquid
146 nitrogen upon removal from the chamber. All spectra were recorded using a microwave frequency of 9.38
147 GHz, a field modulation frequency of 100 kHz, a microwave power of 20.1 mW, a modulation amplitude
148 of 1.0 mT, and a temperature of 23 K.
149
150 **Purification of *A. fulgidus* DsrAB**
151 The purification protocol of the soluble extract from *A. fulgidus* cells followed two consecutive ion
152 exchange chromatography steps at 4 °C under air, as described in detail in Santos *et al.* [7]. The purity of
153 DsrAB was analyzed in a 10% Tricine-SDS-PAGE gel, and the protein concentration was determined by UV-
154 visible spectroscopy using an ε of 60 $mM^{-1}.cm^{-1}$ at 593 nm determined previously [35]. The purified DsrAB

155 was stored under anaerobic conditions to prevent prolonged contact with O_2, which leads to gradual
156 activity loss.
157
158 **Purification of Recombinant *A. fulgidus* DsrC**
159 *A. fulgidus* DsrC with the two structural Cys (Cys^{77} and Cys^{85}) modified to Ala was expressed in *Escherichia*
160 *coli* and purified by an affinity exchange chromatography step on a HiTrap™ immobilized metal-ion affinity
161 chromatography (IMAC) high performance column (GE Healthcare), as described in detail in Ferreira *et al.*
162 [36]. The purity of DsrC was analyzed on a 10% Tricine-SDS-PAGE gel, and the protein concentration was
163 determined by bicinchoninic acid (BCA) assay (Merck Millipore) and by UV-visible spectroscopy using an ε
164 of 24 $mM^{-1}\cdot cm^{-1}$ at 280 nm. Before its use in activity assays, DsrC was treated with 5 mM dithiothreitol
165 (DTT, Sigma-Aldrich) during 30 min at 37 °C, to ensure its Cys were in the reduced state, and excess
166 reductant was removed with a HiTrap™ Desalting column (GE Healthcare) [7]. Reduced DsrC was
167 concentrated, if necessary, by ultrafiltration (10 kDa cutoff, Amicon Millipore) and kept under anaerobic
168 conditions until use. The redox state of the DsrC (5 µg) was analyzed by a gel-shift assay using MalPEG
169 (methoxy-polyethylene glycol maleimide, Fluka), as described in Venceslau *et al.* [37].
170
171 **Production and Analysis of DsrC-trisulfide**
172 The enzymatic production of DsrC-trisulfide was performed inside a Coy anaerobic chamber (98% N_2, 2%
173 H_2) at 60 °C using Zn-reduced methyl viologen (Sigma-Aldrich) as the electron donor [7]. The activity assays
174 were run in 50 mM KPi pH 7.0, 1 mM Zn-reduced methyl viologen (MV^+), 200 nM of DsrAB, 0.5 mM sodium
175 sulfite (Sigma-Aldrich), with a range from 10 µM to 100 µM of reduced DsrC. After a 5 min incubation of
176 DsrAB in the reaction buffer, followed by a 1 min incubation with DsrC, the reaction was started by
177 addition of sodium sulfite. The oxidation of MV^+ was monitored at 732 nm (ε = 3.15 $mM^{-1}\cdot cm^{-1}$) in a
178 spectrophotometer. A prolonged incubation time (from 15 to 60 min depending on the DsrC-trisulfide

179 concentration) was used to try to drive the enzymatic reaction to completion and have DsrC as much as
180 possible in the trisulfide form. The enzymatic solution was diluted and concentrated by ultrafiltration (10
181 kDa cutoff, Amicon Millipore) to remove the methyl viologen. The redox state of DsrC was monitored with
182 the MalPEG gel-shift assay as previously described [37].
183
184 **Determination of DsrC Thiol Content by DTNB**
185 DsrC in different redox states was subject to a DTNB (5,5-dithio-bis-(2-nitrobenzoic acid) – Ellman's
186 reagent) assay to quantify the sulfhydryl groups present. DsrC (0.8 – 3 nmol) was incubated in 100 mM
187 KPi pH 8.0, 1 mM EDTA, and 0.2 mM DTNB (Sigma-Aldrich) for 15 min at room temperature. The
188 production of 2-nitro-5-thiobenzoate anion (TNB^{2-}) was quantified by measuring the absorbance at 412
189 nm using the ε of 14150 $M^{-1}\cdot cm^{-1}$ [38].
190
191 **Surface Plasmon Resonance Analysis**
192 The surface plasmon resonance (SPR) experiments were performed at 25 °C on a BIAcore 2000 instrument
193 (GE Healthcare). DsrC-trisulfide was immobilized on a NTA sensor chip (GE Healthcare) by the His-tag tail
194 present at the N terminus. All the assays were performed with 10 mM HEPES pH 7.4, 150 mM NaCl, 50
195 µM EDTA, and 0.005% (v/v) Tween 20 running buffer. DsrC-trisulfide (45 nM) was bound to a previously
196 activated flow cell at a flow rate of 5 µL/min in the presence of 500 µM $NiCl_2$ in running buffer in order to
197 have an immobilization of around 350 resonance units (RU). Another activated flow cell was similarly
198 treated with running buffer in the absence of DsrC-trisulfide (control cell). Interaction experiments with
199 DsrMKJOP complex were performed with a 3 min injection of increasing concentrations of DsrMKJOP
200 complex (range from 8.9 nM to 568 nM) at a flow rate of 30 µL/min. At the end of sample injection, the
201 NTA sensor chip was regenerated with 350 mM EDTA in running buffer for 1 min at a flow rate of 10
202 µL/min before a new cycle of surface activation and immobilization. Sensorgrams were obtained by

203 subtracting the unspecific binding to the control flow cell in order to remove buffer artifacts and
204 normalizing to the baseline injection timepoint. The equilibrium dissociation constant (K_D) was
205 determined from duplicate experiments and according to $RU_{steady\text{-}state} = (RU_{max} \times [analyte])/K_D + [analyte])$.
206

207 **DsrMKJOP Activity Assays**

208 Menadiol:DsrC-trisulfide oxidoreductase activity assays by DsrMKJOP were performed inside a Coy
209 anaerobic chamber (98% N_2, 2% H_2) at 60 °C using menadiol as electron donor. The activity assays were
210 run in 50 mM KPi pH 7.0, 0.5 mM menadiol, and 100 nM DsrMKJOP in the presence of DsrC-trisulfide (10
211 µM). The reaction was started by addition of DsrC-trisulfide after a 5 min incubation of DsrMKJOP in the
212 reaction buffer. The oxidation of menadiol was monitored at 270 nm (using ε_{DMN} = 16 $mM^{-1} \cdot cm^{-1}$ [39]) in
213 a spectrophotometer. For peptide mass fingerprinting of DsrC, the enzymatic reactions were
214 concentrated and dialyzed by ultrafiltration (10 kDa cutoff, Amicon Millipore). To monitor the redox state
215 of DsrC cysteines, the MalPEG gel-shift assay was used [37].
216

217 **Peptide Mass Fingerprinting**

218 The redox state of DsrC cysteines was analyzed by peptide mass fingerprinting using a matrix-assisted
219 laser desorption/ionization-time-of-flight (MALDI-TOF/TOF) mass spectrometer, as described in Santos *et*
220 *al.* [7]. Alkylation was performed inside an anaerobic chamber by incubation of DsrC with 50 mM
221 iodoacetamide (IA, Sigma-Aldrich) in 50 mM ammonium bicarbonate pH 7.8 during 30 min at 55 °C and
222 run on a 10% Tricine-SDS-PAGE gel (15 µg) under non-reducing conditions. The protein bands were
223 excised, destained and digested with Asp-N (Roche, 20 ng/µL) overnight at 37 °C. This endoproteinase
224 generates a peptide comprising both conserved C-terminal cysteine residues, ^{101}DA**C**RIAGLPKPTG**C**V^{115},
225 with predicted mass of 1500.8 Daltons (Da). The digested peptides were desalted and concentrated using

226 POROS C18 (Empore, 3M) and eluted directly onto the MALDI plate using 1 µL of 5 mg/mL alpha-cyano-4-
227 hydroxycinnamic acid (CHCA, Sigma-Aldrich) in 50% (v/v) acetonitrile and 5% (v/v) formic acid.
228 The data were acquired in positive reflector MS mode using a 5800 MALDI-TOF/TOF (AB Sciex) mass
229 spectrometer and TOF/TOF Series Explorer Software v.4.1.0 (Applied Biosystems). External calibration was
230 performed using CalMix5 (Protea). Mass Spectrometry (MS) data were analyzed using Data Explorer
231 Software v.4.11 (AB Sciex) and obtained at the Mass Spectrometry Unit (UniMS), ITQB/iBET, Oeiras,
232 Portugal.
233
234 **Determination of Hydrogen Sulfide by HPLC**
235 Hydrogen sulfide was quantified using monobromobimane (mBBr) derivatization [40]. mBBr (Thermo
236 Fisher Scientific) was diluted in HPLC ultrapure acetonitrile to a final concentration of 50 mM. For
237 derivatization, 10 µL of sample from the enzymatic reaction were reacted with 3 µL of mBBr in 50 mM
238 EPPS (4-(2-hydroxyethyl)piperazine-1-propanesulfonic acid) pH 8.0 and 5 mM DTPA
239 (diethylenetriaminepentaacetic acid) in a final volume of 86 µL, inside an anaerobic chamber. The
240 reactions were incubated in the dark at room temperature for 10 min, after which 4 µL of 5 M
241 methanesulfonic acid was added to stop the reaction.
242 Derivatized hydrogen sulfide (sulfide dibimane) was measured by high performance liquid
243 chromatography (HPLC, Waters Alliance 2695) with a fluorescence detector (Waters 2475) with an
244 excitation/emission wavelength of 380 and 480 nm, respectively, using a reverse phase Ultrasphere® ODS
245 column (4.6 x 250 mm, 5 µm, Hichrom) run at a flow rate of 1.2 $mL \cdot min^{-1}$ and 35 °C, as described in detail
246 in Santos *et al.* [7]. The retention time was 15.5 min for sulfide dibimane. A calibration curve was
247 performed with freshly prepared solutions of sodium sulfide nonahydrate (Sigma-Aldrich) in 50 mM KPi
248 pH 7.0, reacted with excess mBBr.
249

250 **RESULTS AND DISCUSSION**

251 **DsrMKJOP isolation and reduction with Menadiol**

252 The DsrMKJOP transmembrane complex was purified with DDM as solubilizing detergent from
253 membranes of the thermophilic archaeon *A. fulgidus,* by adapting the protocol previously reported by
254 Mander *et al.* [15]. The DsrMKJOP complex is the only heme-containing membrane complex in *A. fulgidus*
255 [18], which facilitates its purification compared with other sulfate reducers, such as *D. desulfuricans* [10].
256 In *A. fulgidus*, the predicted molecular mass for each subunit of the complex is 38.4 kDa (DsrM, locus tag:
257 AF0501), 64.4 kDa (DsrK, AF0502), 16.7 kDa (DsrJ, AF0503), 30.5 kDa (DsrO, AF0499), and 44.2 kDa (DsrP,
258 AF0500). The purified complex displayed four bands on a Tricine-SDS-PAGE gel (**Figure S1**) with apparent
259 molecular masses of 61, 31, 28, and 17 kDa, in line with the report by Mander *et al.* [15]. The 17 kDa band
260 was identified as a cytochrome *c* (DsrJ) by heme-staining, and the other bands were assigned as DsrK (61
261 kDa), DsrM (31 kDa), DsrO (28 kDa), based on previous identifications [10, 15]. As reported before, DsrP
262 is not detected by SDS-PAGE [10, 15] because it is a highly hydrophobic subunit (ten predicted
263 transmembrane helices), which hinders its migration in the gel.

264 The UV-visible spectrum of the as-purified DsrMKJOP (oxidized state) is dominated by absorption maxima
265 at 280, 410 and 527 nm (**Figure 1A**), confirming the presence of hemes. Upon reduction, the Soret peak
266 shifts to 420 nm, and the β- and α-bands are observed at 524 and 557 nm, respectively, which is in line
267 with previously reported spectra of DsrMKJOP from *A. fulgidus* [15] and *D. desulfuricans* [10]. The α-band
268 is quite broad supporting the presence of hemes *b* and *c*. Addition of menadiol reduced 38% of the total
269 hemes as compared with full reduction by dithionite. This corresponds to approximately two hemes
270 reduced, and since hemes *b* typically have higher redox potentials than hemes *c,* this likely corresponds
271 to the two predicted hemes *b* in the quinone-interacting DsrM membrane subunit. A similar result was
272 reported by Pires *et al.* [10], where 40% of hemes belonging to the *D. desulfuricans* DsrMKJOP were also
273 reduced upon incubation with menadiol.

274 The electron paramagnetic resonance (EPR) spectrum of the as-purified *A. fulgidus* DsrMKJOP shows an
275 intense rhombic signal characteristic of a noncubane $[4Fe\text{-}4S]^{3+/2+}$ cluster in the oxidized state, with *g*-
276 values of 2.025, 1.995 and 1.947 (**Figure 1B**). This EPR signature was first observed in heterodisulfide
277 reductases from methanogens (upon addition of HS-CoM or HS-CoB), with *g*-values of 2.013, 1.991 and
278 1.938 for HdrABC from *Methanothermobacter marburgensis* and 2.012, 1.993 and 1.946 for HdrED from
279 *Methanosarcina barkeri* [41, 42], both of which possess two noncubane $[4Fe\text{-}4S]^{3+/2+}$ catalytic centers
280 involved in mediating heterodisulfide (CoM-S-S-CoB) reduction in two one-electron steps [21, 43]. The
281 previously reported *g*-values of *A. fulgidus* DsrMKJOP were 2.031, 1.994 and 1.941 [15], while in *D.*
282 *desulfuricans* DsrMKJOP the *g*-values were 2.027, 1.991 and 1.943 [10]. Given the similarity of DsrK to
283 HdrD, the noncubane $[4Fe\text{-}4S]^{3+/2+}$ cluster present in DsrK is likely involved in thiol/disulfide chemistry,
284 suggesting that DsrK is the catalytic subunit of the DsrMKJOP complex. Upon incubation with menadiol
285 under anaerobic conditions, the intensity of the rhombic signal decreased by 85%, revealing a pathway
286 for electron transfer from the hemes *b* of DsrM to the noncubane $[4Fe\text{-}4S]^{3+/2+}$ cluster of DsrK. The redox
287 potential of the noncubane center in *A. fulgidus* DsrK was previously determined to be +90 mV [15], which
288 agrees with its reduction by menadiol (midpoint potential of approx. -70 mV).
289
290 **The DsrC-trisulfide interacts strongly with DsrMKJOP**
291 In *A. vinosum*, coelution upon protein purification suggested that DsrK interacts with DsrC [16]. Following
292 our identification of the DsrC-trisulfide as the product of sulfite reduction by DsrAB, we proposed that this
293 is the actual substrate for the DsrMKJOP complex [7]. To assess if there is a protein-protein interaction
294 between the DsrC-trisulfide and the DsrMKJOP complex, surface plasmon resonance (SPR) was initially
295 used. SPR is a highly sensitive technique for studying protein-protein interactions, without the need for
296 labeling. The *A. fulgidus* DsrC-trisulfide was produced by *in vitro* enzymatic reaction using DsrAB from the
297 same organism, as described in Santos *et al.* [7]. The DsrC-trisulfide thus produced was immobilized on a

298 nitrilotriacetic acid (NTA) sensor chip by the N-terminal His-tag, and the interaction was studied with
299 increasing concentrations of DsrMKJOP complex (**Figure 2**). A strong interaction was observed between
300 the two proteins, which could be detected even at low concentrations of the membrane complex. Steady-
301 state conditions could not be achieved (even by increasing the association time), which means that no
302 kinetic model could fit the experimental data, and so the association and dissociation rate constants could
303 not be obtained. Nevertheless, an estimate for the equilibrium dissociation constant (K_D) of 200 ± 27 nM
304 was derived from duplicate sensorgrams using the maximum response reached. This K_D confirms a strong
305 interaction between the DsrC-trisulfide and the DsrMKJOP complex (strong interactions are in the
306 nanomolar range, or even lower as in the case of high-affinity antibodies), supporting the DsrC-trisulfide
307 as a possible substrate for the membrane-bound DsrMKJOP complex. The SPR data were obtained at 25
308 °C, whereas a higher temperature (as used in the activity assays) should favor the association and
309 dissociation rates of DsrC-trisulfide to DsrMKJOP complex since *A. fulgidus* is a thermophile, suggesting
310 that the actual K_D at physiological temperatures may be somewhat different, and possibly even lower.
311
312 **The DsrC-trisulfide is reduced by DsrMKJOP**
313 Given that menadiol can reduce the noncubane $[4Fe\text{-}4S]^{3+/2+}$ catalytic center of DsrK, and that the DsrC-
314 trisulfide interacts with DsrMKJOP complex, we tested whether the DsrC-trisulfide can serve as substrate
315 and electron acceptor for the menadiol-reduced DsrMKJOP complex. Menadiol:DsrC-trisulfide
316 oxidoreductase activity by the DsrMKJOP complex was thus measured. These experiments confirmed a
317 fast oxidation of menadiol (measured by menadione formation at 270 nm) in the presence of the DsrC-
318 trisulfide with a specific activity of 85.5 ± 5.4 mU/mg, assuming DsrMKJOP as a 5-subunit monomer (200
319 kDa) (**Figure 3A**). In control reactions without DsrMKJOP, menadiol or DsrC-trisulfide no activity was
320 detected. In addition, sequential additions of DsrC-trisulfide, after the reaction has stopped, trigger a new
321 phase of menadiol oxidation confirming it had stopped due to substrate depletion (**Figure 3B**).

322 The redox state of DsrC, before and after the reaction, was analyzed by a gel-shift assay using MalPEG,
323 which selectively labels cysteine thiol groups [7, 37]. In this assay, the DsrC-trisulfide presents no shift in
324 the gel as it cannot bind MalPEG, whereas the reduced form binds one or two MalPEG molecules, as the
325 last Cys_A is more accessible for labeling than Cys_B (Cys^{114} and Cys^{103} in *A. fulgidus*, respectively) [7, 37]. At
326 time zero (T_0), most DsrC shows no shift, as expected for the trisulfide, but a small amount of reduced
327 species is present, as revealed by labeling for one MalPEG, due to incomplete production of DsrC-trisulfide
328 by DsrAB (**Figure 3C**). After the enzymatic reaction (T_f), most DsrC is now in the reduced form, as revealed
329 by the shift for one (Cys_A) and two labeled cysteines (Cys_A and Cys_B) (**Figure 3C**). In the control experiments,
330 without DsrMKJOP or menadiol, DsrC remains in the oxidized DsrC-trisulfide state. Using the MalPEG assay
331 to follow the reaction in time, the decrease in the DsrC-trisulfide band and increase in the band for
332 reduced, doubly labeled DsrC, is clearly seen (**Figure 3D**). Increasing concentrations of menadiol for the
333 same reaction time also increase the extent of reaction (**Figure 3E**). As a control, reduced DsrC was tested
334 as a substrate for DsrMKJOP under the same conditions. In this case, no activity is observed (**Figure S2A**),
335 as expected, and the MalPEG assay confirms the reduced state of DsrC in the beginning and end of the
336 experiment (**Figure S2B).**
337 Finally, the redox state of DsrC cysteines was also characterized by peptide mass fingerprinting after
338 protein digestion with Asp-N endoproteinase, which gives rise to a small peptide containing both Cys_A and
339 Cys_B, followed by alkylation with iodoacetamide (IA), which adds 57 Da per reduced cysteine [7]. In
340 reduced DsrC, the C-terminal peptide ^{101}DA**C**RIAGLPKPTG**C**V^{115} has a mass of 1498.7 Da [7], and upon
341 alkylation, a peptide with 1614.9 Da is detected (**Figure 4A**). In the DsrC-trisulfide formed by reaction with
342 DsrAB, the C-terminal peptide shows a mass increase of 32 Da, 1530.7 Da, which remains unaltered by
343 alkylation with IA (**Figure 4B**). A small amount of unreacted IA-labelled DsrC is still detected in this sample
344 (1614.8 Da), as well as a species that does not react with IA (1498.8) and likely corresponds to DsrC with
345 a disulfide bond between the two Cys. It should be noted that the peak intensities are not directly

346 correlated with relative amounts, as they depend on the different ionization properties of each peptide.
347 As expected, analysis of the DsrC peptide after the reaction with DsrMKJOP, reveals the disappearance of
348 the DsrC-trisulfide peak at 1530.7 Da, and the increase of the 1614.8 Da peak characteristic of reduced
349 DsrC, where two cysteines react with IA (**Figure 4C**).
350
351 **Sulfide is the product of DsrMKJOP catalysis**
352 The products of DsrC-trisulfide reduction by the DsrMKJOP complex should be sulfide and reduced DsrC
353 (**Figure 5A**). To quantify the sulfide released during DsrMKJOP catalysis, the reaction was performed with
354 increasing concentrations of DsrC-trisulfide. These kinetic studies showed an increase in the length of the
355 reaction with increasing substrate concentrations (**Figure 5B**), but not an increase in reaction rate. This
356 indicates that the concentrations used are already saturating and that the Michaelis-Menten constant
357 (K_M) for the DsrC-trisulfide is probably in the nM range, in agreement with the measured K_D. The reaction
358 rates slow down as the substrate becomes exhausted. The product sulfide, quantified by HPLC as the
359 monobromobimane fluorescent derivative, increases linearly with increasing DsrC-trisulfide
360 concentrations (**Figure 5C**), although in sub-stoichiometric amounts (40 to 50%). This can be explained by
361 two factors: the partial escape of hydrogen sulfide to the gas phase at pH 7.0, made worse by the high
362 temperature required for the DsrMKJOP assay, and also by a degree of uncertainty associated with
363 quantification of the DsrC-trisulfide. This quantification was performed indirectly using the BCA (for
364 protein quantification) and DTNB (for thiol quantification) assays, by the amount of reduced DsrC
365 remaining in samples of the DsrC-trisulfide. However, we observed by mass spectrometry (MS) that upon
366 production of the DsrC-trisulfide some part of DsrC is in the disulfide state and is not alkylated by IA (peak
367 1498.8 Da in **Figure 4B and 4C**) and thus is also not quantified by DTNB derivatization, generating an
368 uncertainty in the actual level of DsrC-trisulfide present in the samples. Nevertheless, taken globally these

369 results show clearly that DsrMKJOP can catalyze full reduction of the DsrC-trisulfide to sulfide using
370 menadiol, finally clarifying the functional role of this respiratory complex in dissimilatory sulfite reduction.
371

372 **Insights into the catalytic mechanism of DsrMKJOP**

373 A catalytic mechanism for heterodisulfide reduction by Hdrs has been proposed based on the structure of
374 HdrABC with substrate bound, where the CoM-S-S-CoB heterodisulfide binds between the two noncubane
375 $[4Fe\text{-}4S]^{3+/2+}$ clusters and is homolytically cleaved [29]. The thyil radicals formed may be stabilized by
376 coordination with the reduced $[4Fe\text{-}4S]^{2+}$ clusters, leading to the binding of the CoM and CoB sulfurs to
377 the two $[4Fe\text{-}4S]^{3+}$ clusters, resulting in the "open" conformation of the clusters [30]. Two consecutive
378 single-electron reduction steps release CoB-SH and CoM-SH [29, 30]. However, the catalytic mechanism
379 of the DsrMKJOP complex is likely different since it coordinates a single noncubane $[4Fe\text{-}4S]^{3+/2+}$ cluster in
380 DsrK instead of the two found in HdrD and HdrB (**Figure S3**). Interestingly, in many DsrK proteins from
381 different sulfate reducers the last cysteine of the CCG motif for binding this cluster is replaced by a
382 conserved aspartate (**Figure S4**). In *A. fulgidus*, the DsrK protein of the DsrMKJOP complex (AF0502) and
383 another homolog (AF0543) have this aspartate, whereas two other DsrK homologs (AF0544 and AF0547),
384 encoded in *dsrMK* arrangements, have a cysteine, suggesting that both residues may be functional. In
385 addition, one of the conserved cysteines from the missing noncubane cluster (Cys^{329} in *A. fulgidus*
386 numbering) is strictly conserved in DsrK proteins and is likely involved in the catalytic mechanism of DsrC-
387 trisulfide reduction. This cysteine is part of a conserved GECGH sequence motif that is highly conserved in
388 DsrK from several organisms (**Figure S4**) and is one of the cysteines from the second CCG signature motif
389 in HdrD and HdrB (**Figure S3**). A similar motif (ECGLH), present in APS and PAPS reductases, includes a
390 redox-active catalytic cysteine [44]. Other proteins from sulfate reducers, homologous to DsrK and HdrD,
391 such as HmcF from the HmcABCDEF complex [18, 23, 45] and TmcB from the TmcABCD complex [46] also
392 contain only one CCG motif and this conserved cysteine in a T/GECGH motif (**Figure S3**), suggesting that

393 this cysteine is probably essential for disulfide reduction catalysis. The Hmc and Tmc complexes are both
394 transmembrane complexes with a similar architecture to the DsrMKJOP complex, but they are not present
395 in *A. fulgidus* [18]. Interestingly, the characteristic EPR signal of the noncubane $[4Fe\text{-}4S]^{3+}$ cluster was
396 initially reported for the methanogenic HdrB and HdrD only in the presence of HS-CoM or HS-CoB [41–
397 43], which bind to the cluster, whereas for DsrK and TmcB proteins this signal is observed in the as-isolated
398 protein, in the absence of any added substrate [10, 15, 46]. This could suggest that this conserved cysteine
399 might be binding the cluster and generating the open $S = ½$ conformation. However, for the recombinant
400 HdrB protein produced in *E. coli* the signal for the noncubane cluster was visible already in the absence of
401 substrate [22].
402 In methanogens, the redox potential of the CoM-S-S-CoB heterodisulfide has been determined to be $E^{0\prime}$=-
403 143 ± 10 mV vs. SHE [47], which is more positive than that of typical disulfides such as glutathione and
404 cysteine. It is also more positive than the potential of methanophenazine ($E^{0\prime}$=-165 ± 6 mV), the
405 membrane-associated quinone-like redox carrier that is the electron donor to HdrED [47]. The redox
406 potential of the DsrC-trisulfide is unknown, so it is not clear whether its reduction by menaquinol ($E^{0\prime}$ ~ -
407 70 mV) is thermodynamically favorable. Protein disulfide bonds are known to span a wide range of
408 potentials. For example, *A. fulgidus* proteins from the thioredoxin superfamily have potentials ranging
409 from -32 mV to -309 mV (pH 7.0) [48]. A value of -346 mV (pH 7.0, vs. SHE) has been reported for several
410 organic water-soluble trisulfides [49], but we know of no reports for redox potentials of protein-bound
411 trisulfides, so it is very difficult to estimate the redox potential of the DsrC trisulfide. We tested the
412 chemical reduction of this species by different chemical reducing agents, and surprisingly none of them,
413 not even those with very low redox potential, could reduce the DsrC-trisulfide as analyzed with the
414 MalPEG shift assay (**Figure S5**). Moreover, MS confirmed the intact state of the DsrC-trisulfide after
415 reduction with dithionite, TCEP and DTT (**Table S1**). This unexpected result suggests that the DsrC-
416 trisulfide can only be reduced by the DsrMKJOP complex. The fact that it cannot be chemically reduced

417 could suggest that it has a low redox potential, which could increase upon interaction with the DsrMKJOP
418 complex, but it is also possible that the reduction of the trisulfide is not thermodynamically, but kinetically
419 prevented, i.e. that the reaction has a high activation energy and occurs only when it is enzymatically
420 catalyzed. This sort of argument has been put forward by Flohé and coworkers in discussing the
421 glutathione redox potential and its physiological significance [50, 51]. Such kinetic impediment for
422 reduction of the DsrC-trisulfide, which may be based on steric inaccessibility of the trisulfide, makes sense
423 considering that this species is likely to face a considerable intracellular sulfide concentration.
424 Nevertheless, the full reduction of the DsrC-trisulfide, as observed by MS, and the increasing production
425 of sulfide upon reaction of DsrMKJOP and menadiol with increasing concentrations of DsrC-trisulfide
426 confirm that its reduction by this menaquinol analog does occur. This reaction could, in principle, only
427 involve the DsrMK subunits in analogy to HdrED, with DsrM as the menaquinol-oxidizing subunit that
428 transfers electrons to DsrK for trisulfide reduction, and in fact, in many organisms only these two subunits
429 are present [2, 18]. This leaves the function of the DsrJOP subunits as an enigma.
430 It has been suggested that the DsrJ cytochrome could react with a periplasmic sulfur substrate [10, 15,
431 24], due to the presence of the unusual His/Cys heme coordination that is also present in SoxXA involved
432 in thiosulfate oxidation [52] or in TsdA thiosulfate dehydrogenase [26]. We tested both thiosulfate and
433 sulfite as electron donors to the complex and could not detect any activity with menadione and/or DsrC-
434 trisulfide as electron acceptors, and sulfite actually decreased the rate of DsrC-trisulfide reduction by
435 DsrMKJOP (**Figure S6**). Since the DsrJOP module is not essential for some organisms, a hypothesis is that
436 its role is to increase the energetic efficiency of the DsrMKJOP complex vs. the DsrMK version. We have
437 previously suggested that the DsrMK and DsrJOP modules could be involved in some form of proton-
438 translocating quinone cycling, as present in the bc_1 complex, possibly involving quinone-based electron
439 bifurcation [9]. Alternatively, the DsrJOP module may allow for proton pumping upon DsrC-trisulfide
440 reduction. Notably, the DsrOP proteins form a quinone-interacting redox module that is widespread in

441 bacterial oxidoreductases [23, 53], and some proteins of the DsrP family may be involved in proton
442 pumping, such as the alternative complex III [54, 55] and the reductive dehalogenase complex [56].

443 **CONCLUSION**

444 In conclusion, our results are a major step forward in the molecular understanding of dissimilatory sulfur
445 metabolism by identifying the function of the DsrMKJOP complex, showing that it interacts with the DsrC-
446 trisulfide and acts as a menadiol:DsrC-trisulfide oxidoreductase that produces sulfide. The architecture of
447 the DsrMKJOP complex indicates that it is quite an elaborate machine and clearly more detailed
448 biochemical and structural studies will be essential to understand its molecular mechanism and how it is
449 coupled to energy conservation.

450

451 **ACKNOWLEDGEMENTS**

452 We thank João Carita and Cristina Leitão from ITQB NOVA for the growth of *A. fulgidus* and HPLC analysis,
453 respectively. This work was funded by the Fundação para a Ciência e Tecnologia (Portugal) through
454 Fellowships PD/BD/135488/2018 and COVID/BD/152504/2022 (A.C.C.B.), Grants PTDC/BIA-
455 MIC/6512/2014 and PTDC/BIA-BQM/29118/2017, Research Unit Molecular, Structural and Cellular
456 Microbiology (MOSTMICRO-ITQB) (UIDB/04612/2020 and UIDP/04612/2020), and Associate Laboratory
457 Life Sciences for a Healthy and Sustainable Future (LS4FUTURE) (LA/P/0087/2020).

458

459 **AUTHOR CONTRIBUTIONS**

460 S.S.V. and I.A.C.P. designed research; A.C.C.B. and S.S.V. performed research; A.C.C.B., S.S.V. and I.A.C.P.
461 analyzed data; A.C.C.B., S.S.V. and I.A.C.P. wrote the paper.

462 The authors have no competing interests.

463

464 **Data Availability Statement:**

465 The raw data is available from the authors upon request.

466 **REFERENCES**

467 1. Muyzer G, Stams AJM. The ecology and biotechnology of sulphate-reducing bacteria. *Nat Rev*
468 *Microbiol* 2008; **6**: 441–454.

469 2. Rabus R, Venceslau SS, Wöhlbrand L, Voordouw G, Wall JD, Pereira IAC. A Post-Genomic View of
470 the Ecophysiology, Catabolism and Biotechnological Relevance of Sulphate-Reducing Prokaryotes.
471 *Adv Microb Physiol* 2015; **66**: 55–321.

472 3. Jørgensen BB, Findlay AJ, Pellerin A. The biogeochemical sulfur cycle of marine sediments. *Front*
473 *Microbiol* 2019; **10**: 1–27.

474 4. McGlynn SE, Chadwick GL, Kempes CP, Orphan VJ. Single cell activity reveals direct electron
475 transfer in methanotrophic consortia. *Nature* 2015; **526**: 531–535.

476 5. Wegener G, Krukenberg V, Riedel D, Tegetmeyer HE, Boetius A. Intercellular wiring enables
477 electron transfer between methanotrophic archaea and bacteria. *Nature* 2015; **526**: 587–590.

478 6. Canfield DE, Rosing MT, Bjerrum C. Early anaerobic metabolisms. *Philos Trans R Soc B Biol Sci* 2006;
479 **361**: 1819–1836.

480 7. Santos AA, Venceslau SS, Grein F, Leavitt WD, Dahl C, Johnston DT, et al. A protein trisulfide couples
481 dissimilatory sulfate reduction to energy conservation. *Science* 2015; **350**: 1541–1545.

482 8. Oliveira TF, Vonrhein C, Matias PM, Venceslau SS, Pereira IAC, Archer M. The crystal structure of
483 *Desulfovibrio vulgaris* dissimilatory sulfite reductase bound to DsrC provides novel insights into the
484 mechanism of sulfate respiration. *J Biol Chem* 2008; **283**: 34141–34149.

485 9. Venceslau SS, Stockdreher Y, Dahl C, Pereira IAC. The 'bacterial heterodisulfide' DsrC is a key
486 protein in dissimilatory sulfur metabolism. *Biochim Biophys Acta - Bioenerg* 2014; **1837**: 1148–
487 1164.

488 10. Pires RH, Venceslau SS, Morais F, Teixeira M, Xavier A V., Pereira IAC. Characterization of the
489 *Desulfovibrio desulfuricans* ATCC 27774 DsrMKJOP complex - A membrane-bound redox complex

490 involved in the sulfate respiratory pathway. *Biochemistry* 2006; **45**: 249–262.

491 11. Pott AS, Dahl C. Sirohaem sulfite reductase and other proteins encoded by genes at the dsr locus
492 of *Chromatium vinosum* are involved in the oxidation of intracellular sulfur. *Microbiology* 1998;
493 **144**: 1881–1894.

494 12. Dahl C. A biochemical view on the biological sulfur cycle. In: Piet N. L. Lens (ed.). Environmental
495 Technologies to Treat Sulfur Pollution: Principles and Engineering. IWA Publishing, 2020; pp 55–
496 96.

497 13. Simon J, Kroneck PMH. Microbial Sulfite Respiration. *Adv Microb Physiol* 2013; **62**: 45–117.

498 14. Wasmund K, Mußmann M, Loy A. The life sulfuric: microbial ecology of sulfur cycling in marine
499 sediments. *Environ Microbiol Rep* 2017; **9**: 323–344.

500 15. Mander GJ, Duin EC, Linder D, Stetter KO, Hedderich R. Purification and characterization of a
501 membrane-bound enzyme complex from the sulfate-reducing archaeon *Archaeoglobus fulgidus*
502 related to heterodisulfide reductase from methanogenic archaea. *Eur J Biochem* 2002; **269**: 1895–
503 1904.

504 16. Grein F, Pereira IAC, Dahl C. Biochemical characterization of individual components of the
505 *Allochromatium vinosum* DsrMKJOP transmembrane complex aids understanding of complex
506 function in vivo. *J Bacteriol* 2010; **192**: 6369–6377.

507 17. Sander J, Engels-Schwarzlose S, Dahl C. Importance of the DsrMKJOP complex for sulfur oxidation
508 in *Allochromatium vinosum* and phylogenetic analysis of related complexes in other prokaryotes.
509 *Arch Microbiol* 2006; **186**: 357–366.

510 18. Pereira IAC, Ramos AR, Grein F, Marques MC, da Silva SM, Venceslau SS. A comparative genomic
511 analysis of energy metabolism in sulfate reducing bacteria and archaea. *Front Microbiol* 2011; **2**:
512 25–36.

513 19. Heiden S, Hedderich R, Setzke E, Thauer RK. Purification of a two-subunit cytochrome-*b*-containing

514 heterodisulfide reductase from methanol-grown *Methanosarcina barkeri*. *Eur J Biochem* 1994;
515 **221**: 855–861.
516 20. Künkel A, Vaupel M, Heim S, Thauer RK, Hedderich R. Heterodisulfide reductase from methanol-
517 grown cells of *Methanosarcina barkeri* is not a flavoenzyme. *Eur J Biochem* 1997; **244**: 226–234.
518 21. Hedderich R, Hamann N, Bennati M. Heterodisulfide reductase from methanogenic archaea: A new
519 catalytic role for iron-sulfur cluster. *Biol Chem* 2005; **386**: 961–970
520 22. Hamann N, Mander GJ, Shokes JE, Scott RA, Bennati M, Hedderich R. A cysteine-rich CCG domain
521 contains a novel [4Fe-4S] cluster binding motif as deduced from studies with subunit B of
522 heterodisulfide reductase from Methanothermobacter marburgensis. *Biochemistry* 2007; **46**:
523 12875–12885.
524 23. Duarte AG, Barbosa ACC, Ferreira D, Manteigas G, Domingos RM, Pereira IAC. Redox loops in
525 anaerobic respiration - The role of the widespread NrfD protein family and associated dimeric
526 redox module. *Biochim Biophys Acta - Bioenerg* 2021; **1862**: 148416.
527 24. Grein F, Venceslau SS, Schneider L, Hildebrandt P, Todorovic S, Pereira IAC, et al. DsrJ, an essential
528 part of the DsrMKJOP transmembrane complex in the purple sulfur bacterium *Allochromatium*
529 *vinosum*, is an unusual triheme cytochrome c. *Biochemistry* 2010; **49**: 8290–8299.
530 25. Cheesman MR, Little PJ, Berks BC. Novel heme ligation in a *c*-type cytochrome involved in
531 thiosulfate oxidation: EPR and MCD of SoxAX from *Rhodovulum sulfidophilum*. *Biochemistry* 2001;
532 **40**: 10562–10569.
533 26. Denkmann K, Grein F, Zigann R, Siemen A, Bergmann J, van Helmont S, et al. Thiosulfate
534 dehydrogenase: A widespread unusual acidophilic *c*-type cytochrome. *Environ Microbiol* 2012; **14**:
535 2673–2688.
536 27. Alric J, Tsukatani Y, Yoshida M, Matsuura K, Shimada K, Hienerwadel R, et al. Structural and
537 functional characterization of the unusual triheme cytochrome bound to the reaction center of

538 *Rhodovulum sulfidophilum*. *J Biol Chem* 2004; **279**: 26090–26097.

539 28. Grein F, Ramos AR, Venceslau SS, Pereira IAC. Unifying concepts in anaerobic respiration: Insights
540 from dissimilatory sulfur metabolism. *Biochim Biophys Acta - Bioenerg* . 2013; **1827**: 145–160

541 29. Wagner T, Koch J, Ermler U, Shima S. Methanogenic heterodisulfide reductase (HdrABC-MvhAGD)
542 uses two noncubane [4Fe-4S] clusters for reduction. *Science* 2017; **357**: 699–703.

543 30. Pelmenschikov V, Ferreira D, Venceslau SS, Hildebrandt P, Pereira IAC, Todorovic S. Substrate-
544 Dependent Conformational Switch of the Noncubane [4Fe-4S] Cluster in Heterodisulfide Reductase
545 HdrB. *J Am Chem Soc* 2023; **145**: 7–11.

546 31. Stetter KO, Lauerer G, Thomm M, Neuner A. Isolation of Extremely Thermophilic Sulfate Reducers:
547 Evidence for a Novel Branch of Archaebacteria. *Science* 1987; **236**: 822–824.

548 32. Francis RT, Becker RR. Specific indication of hemoproteins in polyacrylamide gels using a double-
549 staining process. *Anal Biochem* 1984; **136**: 509–514.

550 33. Venceslau SS. Electron transfer chains in sulfate reducing bacteria. Instituto de Tecnologia Química
551 e Biológica António Xavier, Universidade Nova de Lisboa. Ph.D. Thesis Dissertation 2011.

552 34. Fieser LF. Convenient Procedures for the Preparation of Antihemorrhagic Compounds. *J Biol Chem*
553 1940; **133**: 391–396.

554 35. Dahl C, Kredich NM, Deutzmann R, Truper HG. Dissimilatory sulphite reductase from
555 *Archaeoglobus fulgidus*: Physico-chemical properties of the enzyme and cloning, sequencing and
556 analysis of the reductase genes. *J Gen Microbiol* 1993; **139**: 1817–1828.

557 36. Ferreira D, Barbosa ACC, Oliveira GP, Catarino T, Venceslau SS, Pereira IAC. The DsrD functional
558 marker protein is an allosteric activator of the DsrAB dissimilatory sulfite reductase. *Proc Natl Acad*
559 *Sci USA* 2022; **119**.

560 37. Venceslau SS, Cort JR, Baker ES, Chu RK, Robinson EW, Dahl C, et al. Redox states of *Desulfovibrio*
561 *vulgaris* DsrC, a key protein in dissimilatory sulfite reduction. *Biochem Biophys Res Commun* 2013;

562 **441**: 732–736.

563 38. Riddles PW, Blakeley RL, Zerner B. Reassessment of Ellman's Reagent. *Methods Enzymol* 1983; **91**:
564 49–60.

565 39. Weiner JH, Cammack R, Cole ST, Condon C, Honoré N, Lemire BD, et al. A mutant of *Escherichia*
566 *coli* fumarate reductase decoupled from electron transport. *Proc Natl Acad Sci* 1986; **83**: 2056–
567 2060.

568 40. Fahey RC, Newton GL. Determination of Low-Molecular-Weight Thiols using Monobromobimane
569 Fluorescent Labeling and High-Performance Liquid Chromatography. *Methods Enzymol* 1987; **143**:
570 85–96.

571 41. Madadi-Kahkesh S, Duin EC, Heim S, Albracht SPJ, Johnson MK, Hedderich R. A paramagnetic
572 species with unique EPR characteristics in the active site of heterodisulfide reductase from
573 methanogenic archaea. *Eur J Biochem* 2001; **268**: 2566–2577.

574 42. Duin EC, Bauer C, Jaun B, Hedderich R. Coenzyme M binds to a [4Fe-4S] cluster in the active site of
575 heterodisulfide reductase as deduced from EPR studies with the [^{33}S]coenzyme M-treated enzyme.
576 *FEBS Lett* 2003; **538**: 81–84.

577 43. Duin EC, Madadi-Kahkesh S, Hedderich R, Clay MD, Johnson MK. Heterodisulfide reductase from
578 *Methanothermobacter marburgensis* contains an active-site [4Fe-4S] cluster that is directly
579 involved in mediating heterodisulfide reduction. *FEBS Lett* 2002; **512**: 263–268.

580 44. Bhave DP, Hong JA, Keller RL, Krebs C, Carroll KS. Iron-sulfur cluster engineering provides insight
581 into the evolution of substrate specificity among sulfonucleotide reductases. *ACS Chem Biol* 2012;
582 **7**: 306–315.

583 45. Rossi M, Pollock WBR, Reij MW, Keon RG, Fu R, Voordouw G. The hmc operon of *Desulfovibrio*
584 *vulgaris* subsp. *vulgaris* Hildenborough encodes a potential transmembrane redox protein
585 complex. *J Bacteriol* 1993; **175**: 4699–4711.

586 46. Pereira PM, Teixeira M, Xavier A V., Louro RO, Pereira IAC. The Tmc complex from *Desulfovibrio*
587 *vulgaris* Hildenborough is involved in transmembrane electron transfer from periplasmic hydrogen
588 oxidation. *Biochemistry* 2006; **45**: 10359–10367.
589 47. Tietze M, Beuchle A, Lamla I, Orth N, Dehler M, Greiner G, et al. Redox potentials of
590 methanophenazine and CoB-S-S-CoM, factors involved in electron transport in methanogenic
591 archaea. *ChemBioChem* 2003; **4**: 333–335.
592 48. Chobot SE, Hernandez HH, Drennan CL, Elliott SJ. Direct Electrochemical Characterization of
593 Archaeal Thioredoxins. *Angew Chemie Int Ed* 2007; **46**: 4145–4147.
594 49. Zöphel A, Kennedy MC, Beinert H, Kroneck PMH. Investigations on microbial sulfur respiration.
595 *Arch Microbiol* 1988; **150**: 72–77.
596 50. Flohé L. The fairytale of the GSSG/GSH redox potential. *Biochim Biophys Acta - Gen Subj* 2013;
597 **1830**: 3139–3142.
598 51. Berndt C, Lillig CH, Flohé L. Redox regulation by glutathione needs enzymes. *Front Pharmacol* 2014;
599 **5**.
600 52. Bamford VA, Bruno S, Rasmussen T, Appia-Ayme C, Cheesman MR, Berks BC, et al. Structural basis
601 for the oxidation of thiosulfate by a sulfur cycle enzyme. *EMBO J* 2002; **21**: 5599–5610.
602 53. Duarte AG, Catarino T, White GF, Lousa D, Neukirchen S, Soares CM, et al. An electrogenic redox
603 loop in sulfate reduction reveals a likely widespread mechanism of energy conservation. *Nat*
604 *Commun* 2018; **9**: 5448.
605 54. Sousa JS, Calisto F, Langer JD, Mills DJ, Refojo PN, Teixeira M, et al. Structural basis for energy
606 transduction by respiratory alternative complex III. *Nat Commun* 2018; **9**: 1728.
607 55. Sun C, Benlekbir S, Venkatakrishnan P, Wang Y, Hong S, Hosler J, et al. Structure of the alternative
608 complex III in a supercomplex with cytochrome oxidase. *Nature* 2018; **557**: 123–126.
609 56. Kublik A, Deobald D, Hartwig S, Schiffmann CL, Andrades A, von Bergen M, et al. Identification of a

610 multi-protein reductive dehalogenase complex in *Dehalococcoides mccartyi* strain CBDB1 suggests
611 a protein-dependent respiratory electron transport chain obviating quinone involvement. *Environ*
612 *Microbiol* 2016; **18**: 3044–3056.
613

614 ## Figure Legends

615 **Figure 1 – UV-visible and EPR spectroscopy of the *A. fulgidus* DsrMKJOP complex.** (A) UV-visible spectra
616 of as-purified DsrMKJOP (black), menadiol-reduced (dark grey), and dithionite-reduced (light grey). (B)
617 EPR spectra of the $[4Fe\text{-}4S]^{3+/2+}$ cluster of the as-purified DsrMKJOP (black), and upon menadiol reduction
618 (grey). *g*-values are marked in the spectrum of as-purified DsrMKJOP. All menadiol reduction spectra were
619 obtained in a 1:500 protein to menadiol ratio.

620

621 **Figure 2 – Interaction assays between DsrC-trisulfide and DsrMKJOP complex.** Sensorgrams of DsrC-
622 trisulfide interaction with increasing concentrations of DsrMKJOP (8.9 nM to 568 nM) using SPR.
623 Sensorgrams were measured in duplicate.

624

625 **Figure 3 – Kinetic assays of the effect of DsrC-trisulfide on DsrMKJOP activity.** (A) Menadiol:DsrC-
626 trisulfide oxidoreductase activity catalyzed by *A. fulgidus* DsrMKJOP (black), and in the absence of DsrC-
627 trisulfide (light grey), absence of DsrMKJOP (dashed line), and absence of menadiol (dotted line). (B)
628 Menadiol:DsrC-trisulfide oxidoreductase activity catalyzed by *A. fulgidus* DsrMKJOP upon successive
629 additions of DsrC-trisulfide (arrow indicates addition of 5 µM DsrC-trisulfide). (C and D) Gel-shift analysis
630 of MalPEG-labeled DsrC from (A) and after reaction with DsrMKJOP and 0.5 mM menadiol over time (at
631 0, 1, 2, 3, 5, 10, 15, 20 and 30 min), respectively. MalPEG causes a shift of approximately 10 kDa per each
632 labeled cysteine. (E) Gel-shift analysis of MalPEG-labeled DsrC with increasing concentrations of menadiol
633 (0, 0.8, 4, 20, 100 and 500 µM), reacted for 30 mins. (M, molecular marker; T_0, time zero; T_f, time at the
634 end of reaction).

635

636 **Figure 4 – Peptide mass fingerprinting spectra of DsrC C-terminal peptides after alkylation with IA.** (A)
637 DTT-reduced DsrC (before the reaction with *A. fulgidus* DsrAB and sulfite). (B) DsrC-trisulfide (produced in

638 the *in vitro* enzymatic reaction with *A. fulgidus* DsrAB and sulfite). (C) DsrC recovered after the *in vitro*
639 enzymatic reaction with *A. fulgidus* DsrMKJOP complex and menadiol. The C-terminal peptide of DsrC-
640 trisulfide (1530.7 Da) is marked with an arrow in (C) showing its disappearance from (B) to (C). (IA,
641 iodoacetamide; DTT, dithiothreitol).

642

643 **Figure 5 – Kinetic assays of the effect of DsrC-trisulfide on DsrMKJOP activity and sulfide production.** (A)
644 Schematic representation of menadiol:DsrC-trisulfide oxidoreductase activity catalyzed by *A. fulgidus*
645 DsrMKJOP. (B) Menadiol:DsrC-trisulfide oxidoreductase activity catalyzed by *A. fulgidus* DsrMKJOP with
646 increasing concentrations of DsrC-trisulfide (0 µM to 10 µM). (C) Hydrogen sulfide measured by HPLC with
647 increasing concentrations of DsrC-trisulfide (0 µM to 10 µM) after 30 min of enzymatic reaction.

648

649

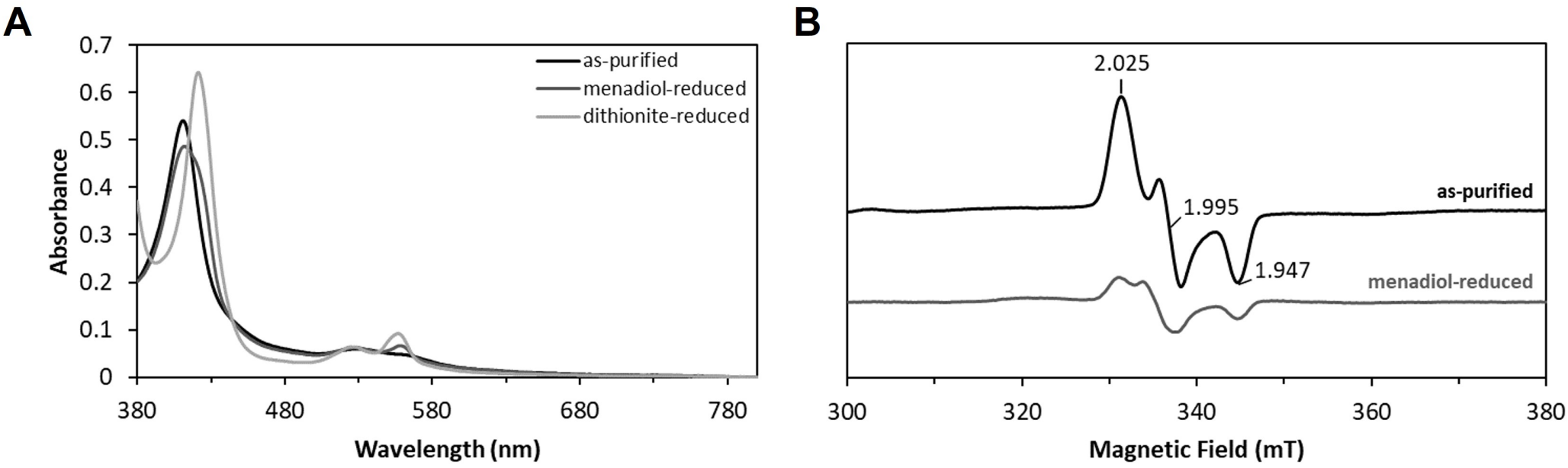
A
0.7
0.6
0.5
0.4
0.3
0.2
0.1
0
Absorbance
380
480
580
680
780
Wavelength (nm)
as-purified
menadiol-reduced
dithionite-reduced
B
2.025
1.995
1.947
as-purified
menadiol-reduced
300
320
340
360
380
Magnetic Field (mT)

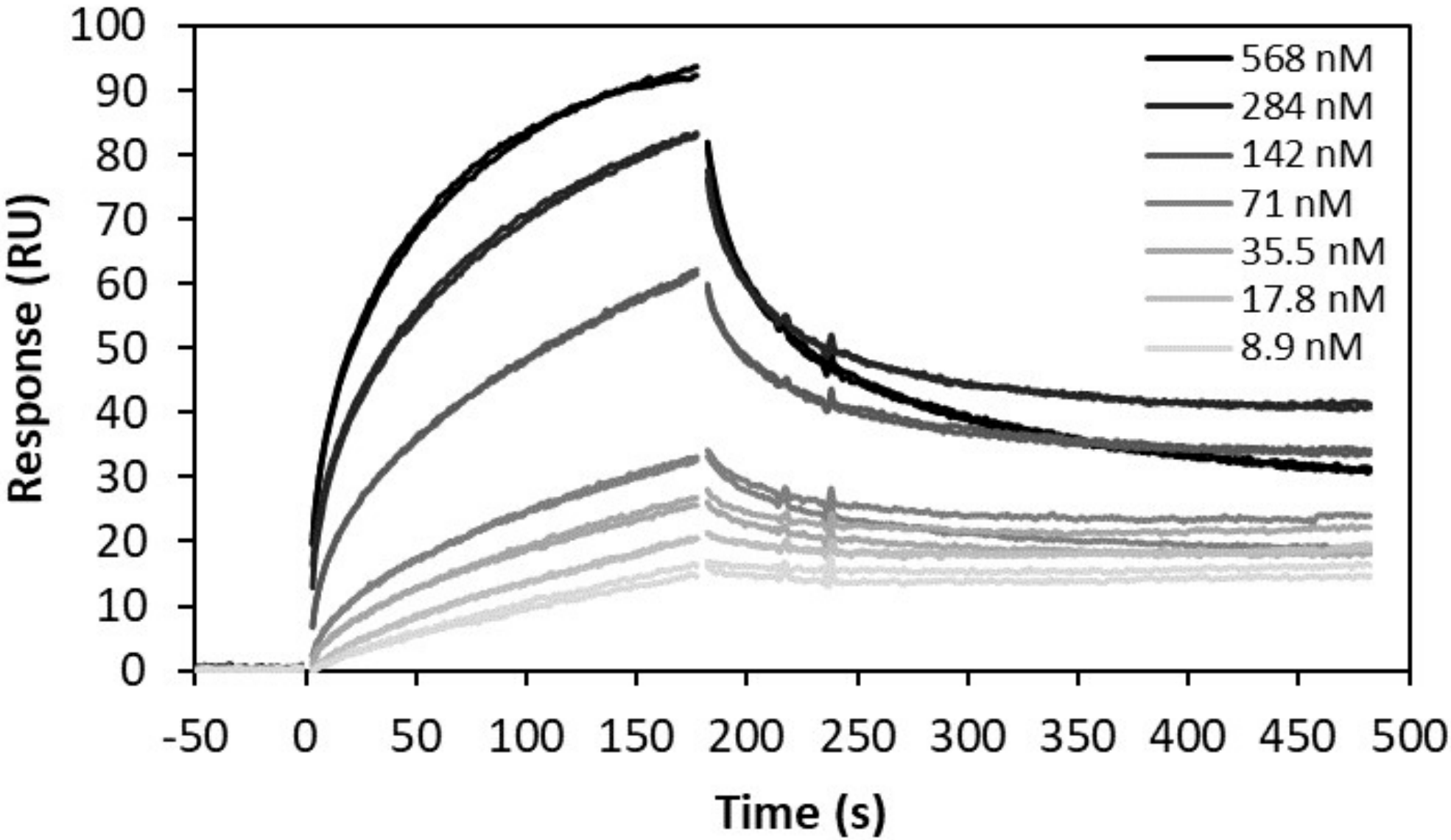
Response (RU)
100
90
80
70
60
50
40
30
20
10
0
-50
0
50
100
150
200
250
300
350
400
450
500
Time (s)
568 nM
284 nM
142 nM
71 nM
35.5 nM
17.8 nM
8.9 nM

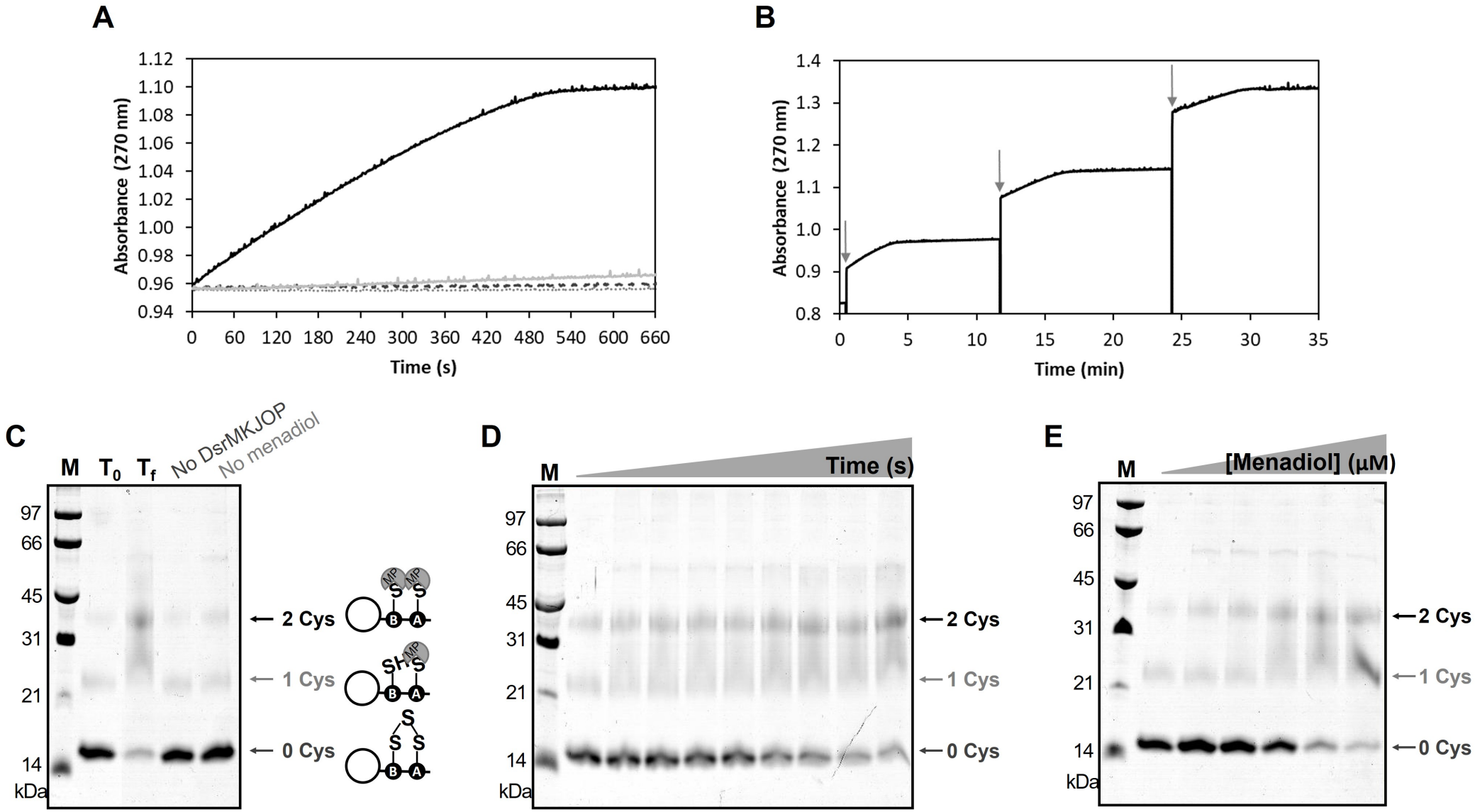
A
Absorbance (270 nm)
Time (s)
B
Absorbance (270 nm)
Time (min)
C
M
T_0
T_f
No DsrMKJOP
No menadiol
2 Cys
1 Cys
0 Cys
kDa
D
M
Time (s)
2 Cys
1 Cys
0 Cys
kDa
E
M
[Menadiol] (µM)
2 Cys
1 Cys
0 Cys
kDa

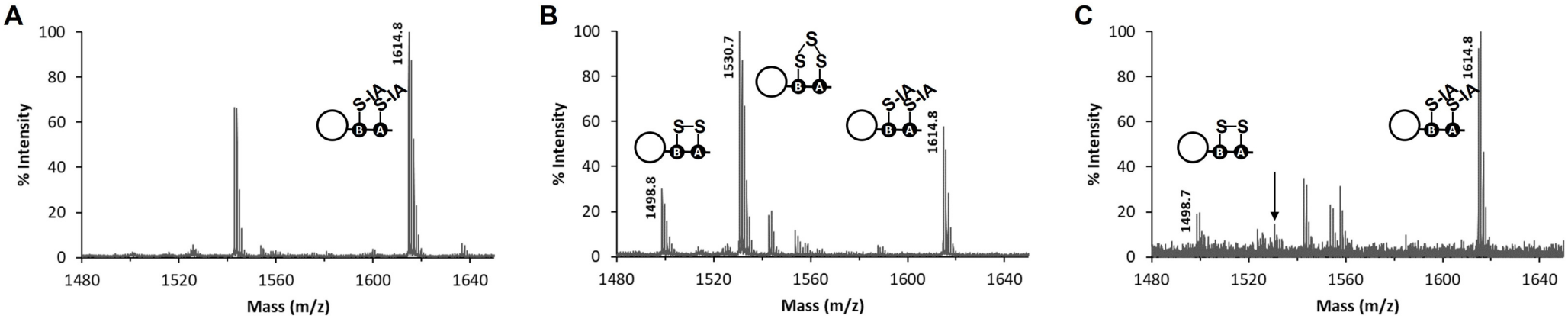
A
B
C
% Intensity
Mass (m/z)
1614.8
1530.7
1498.8
1498.7
S-IA
S
B
A

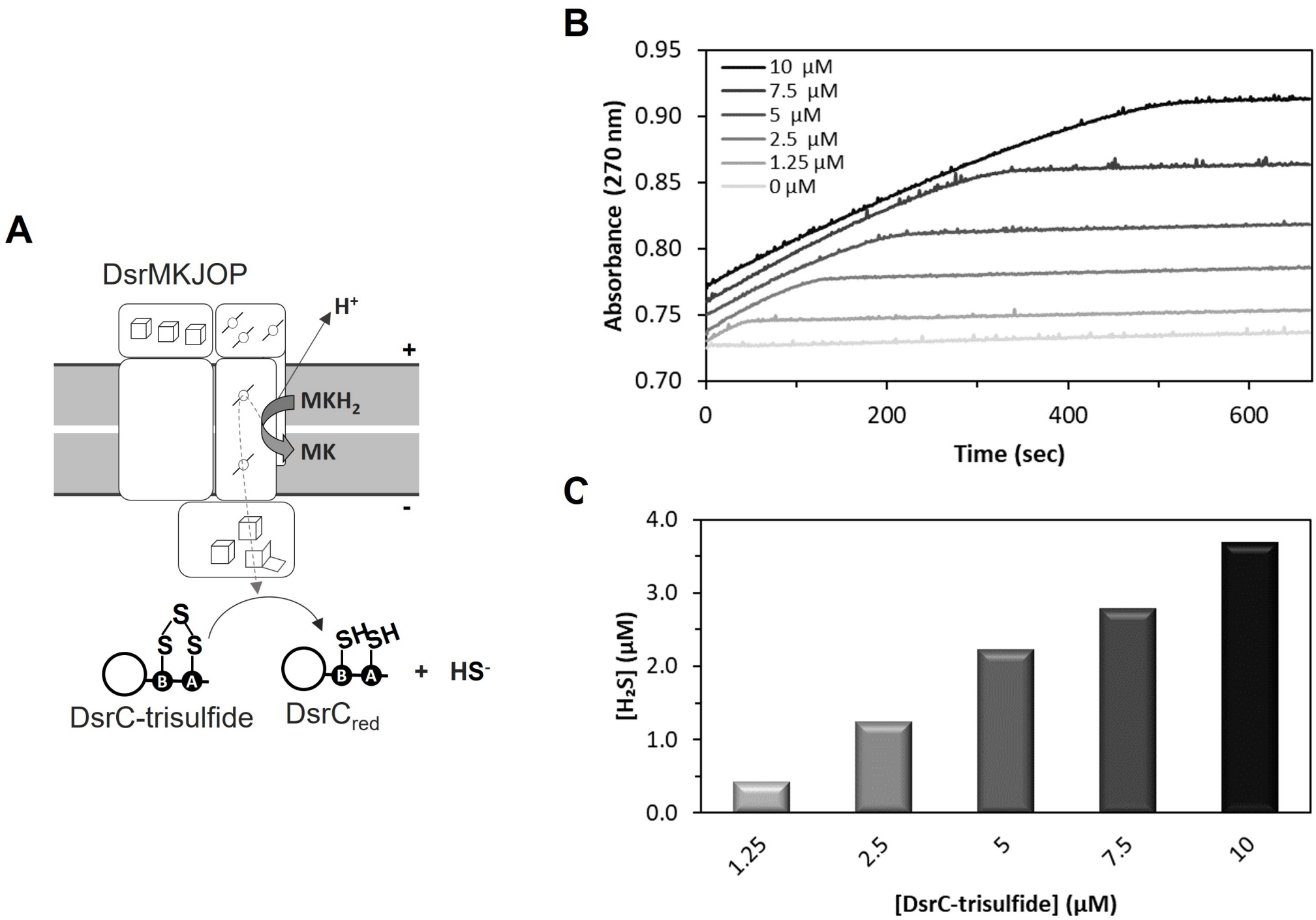
A
DsrMKJOP
H+
+
MKH2
MK
-
S
S S
B A
DsrC-trisulfide
SH SH
B A
DsrCred
+ HS-
B
10 µM
7.5 µM
5 µM
2.5 µM
1.25 µM
0 µM
Absorbance (270 nm)
0.95
0.90
0.85
0.80
0.75
0.70
0
200
400
600
Time (sec)
C
[H2S] (µM)
4.0
3.0
2.0
1.0
0.0
1.25
2.5
5
7.5
10
[DsrC-trisulfide] (µM)